

# A genetically encoded biosensor reveals spatiotemporal variation in cellular phosphate content in *Brachypodium distachyon* mycorrhizal roots

Shiqi Zhang<sup>1</sup> , Dierdra A. Daniels<sup>1\*</sup> , Sergey Ivanov<sup>1\*</sup> , Lucas Jurgensen<sup>1\*</sup>, Lena M. Müller<sup>1\*</sup> , Wayne K. Versaw<sup>2</sup>  and Maria J. Harrison<sup>1</sup> 

<sup>1</sup>Boyce Thompson Institute, 533 Tower Road, Ithaca, NY 14853, USA; <sup>2</sup>Department of Biology, Texas A&M University, College Station, TX 77843, USA

## Summary

Author for correspondence:  
Maria J. Harrison  
Email: [mjh78@cornell.edu](mailto:mjh78@cornell.edu)

Received: 9 November 2021  
Accepted: 28 February 2022

New Phytologist (2022) 234: 1817–1831  
doi: 10.1111/nph.18081

**Key words:** <sup>32</sup>Pi tracing, arbuscules, fluorescence resonance energy transfer (FRET), live imaging, plastids, symbiosis.

- Arbuscular mycorrhizal (AM) symbiosis is accompanied by alterations to root cell metabolism and physiology, and to the pathways of orthophosphate (Pi) entry into the root, which increase with Pi delivery to cortical cells via arbuscules. How AM symbiosis influences the Pi content and Pi response dynamics of cells in the root cortex and epidermis is unknown.
- Using fluorescence resonance energy transfer (FRET)-based Pi biosensors, we mapped the relative cytosolic and plastidic Pi content of *Brachypodium distachyon* mycorrhizal root cells, analyzed responses to extracellular Pi and traced extraradical hyphae-mediated Pi transfer to colonized cells.
- Colonized cortical cells had a higher cytosolic Pi content relative to noncolonized cortical and epidermal cells, while plastidic Pi content was highest in cells at the infection front. Pi application to the entire mycorrhizal root resulted in transient changes in cytosolic Pi that differed in direction and magnitude depending on cell type and arbuscule status; cells with mature arbuscules showed a substantial transient increase in cytosolic Pi while those with collapsed arbuscules showed a decrease. Directed Pi application to extraradical hyphae resulted in measurable changes in cytosolic Pi of colonized cells 18 h after application.
- Our experiments reveal that cells within a mycorrhizal root vary in Pi content and Pi response dynamics.

## Introduction

Phosphorus (P) is one of the macronutrients essential for plant growth and required by all plant cells. It is obtained, mainly in the form of orthophosphate (Pi), from the soil solution by phosphate transporters in the plasma membranes of root epidermal cells. Subsequent distribution to all cells of the plant and to many sub-cellular compartments, is enabled by several additional families of phosphate transporter proteins (Gu *et al.*, 2016; Versaw & Garcia, 2017). Pi is challenging for plants to obtain as P is highly reactive and forms sparingly soluble complexes in the soil. As a consequence, Pi levels in the soil solution are generally low and particularly depleted in the rhizosphere as a result of rapid Pi uptake by roots (Schachtman *et al.*, 1998). Many plants increase their access to Pi through symbiotic associations with arbuscular mycorrhizal (AM) fungi (Chiu & Paszkowski, 2019), a trait that occurs in over 72% of flowering plants (Brundrett, 2017).

During AM symbiosis, the fungal symbiont colonizes the root and also the surrounding soil. This results in hyphal continuity

between the soil and the root cortex which enables Pi delivery to the interior of the root. Symbiotic Pi acquisition starts with Pi uptake by the hyphae in the soil and high-affinity Pi transporters are presumed to mediate this step (Harrison & Buuren, 1995; Maldonado-Mendoza *et al.*, 2001; Xie *et al.*, 2013, 2016). The current models propose that Pi is then assimilated into polyphosphates in vacuoles and translocated through the hyphae to specialized, highly branched hyphae called arbuscules, which are located in the cortical cells (Cox *et al.*, 1980; Rasmussen *et al.*, 2000; Hijikata *et al.*, 2010). Polyphosphate breakdown in the arbuscules is followed by Pi efflux from the fungus. Each arbuscule is surrounded by a plant membrane, the periarbuscular membrane, which contains Pi transporters that transport the fungal-delivered Pi into the root cortical cell (Javot *et al.*, 2007; Yang *et al.*, 2012). In some situations, plants can obtain the majority of their Pi via their fungal symbiont (Smith *et al.*, 2003). The plant supports the AM fungus with lipids and sugar which are synthesized in the colonized cell and exported across the periarbuscular membrane (Bravo *et al.*, 2017; Jiang *et al.*, 2017; Keymer *et al.*, 2017; An *et al.*, 2019). Thus the colonized cortical cells show substantial alterations to their metabolism, cellular organization and physiology.

\*These authors are co-second authors.

In *Brachypodium distachyon* roots, AM fungal hyphae follow an intracellular growth pattern in which thick linear hyphae grow cell to cell along the longitudinal axis of the root (Hong *et al.*, 2012). Arbuscules develop on branches that arise from these thick linear hyphae. Distinct stages can be observed, including arbuscules with a few thick branches, mature arbuscules with many fine branches, and degenerating arbuscules that ultimately form clumps (Gutjahr & Parniske, 2013). These stages can generally be observed consecutively behind the growing hyphal front (Cox & Sanders, 1974; Walker & Smith, 1984). As arbuscules and the periarbuscular membrane develop, the location and morphology of several plant cells organelles are altered. In particular, plastids become highly stromulated, a morphology that has been suggested to be associated with increased metabolic activity (Kwok & Hanson, 2004; Waters *et al.*, 2004), potentially the result of extensive fatty acid biosynthesis.

Several techniques have been used to measure or image Pi levels in plants, such as phosphorus-31 nuclear magnetic resonance ( $^{31}\text{P}$ -NMR), X-ray spectrometry, and use of Pi radioisotopes (Kanno *et al.*, 2016). However, none of these techniques allow *in vivo* monitoring of Pi profiles with cellular resolution in real-time. In contrast, genetically-encoded fluorescent biosensors provide an opportunity to report ion levels as measurable fluorescent signals (Lalonde *et al.*, 2005; Okumoto *et al.*, 2012). Fluorescence resonance energy transfer (FRET)-based biosensors have been widely used to measure ions, such as calcium ion ( $\text{Ca}^{2+}$ ) and zinc ion ( $\text{Zn}^{2+}$ ), and provided new insights that could not have been obtained by other means, such as the discovery of salt stress-induced  $\text{Ca}^{2+}$  waves in *Arabidopsis* roots (Choi *et al.*, 2014). With the development of a series of FRET-based Pi sensors (FLIPPi), it became possible to monitor Pi in real-time as demonstrated in *Cos-7* cells (Gu *et al.*, 2006). Mukherjee *et al.* (2015) improved the dynamic range of these sensors by substituting enhanced yellow fluorescent protein (eYFP) with circularly permuted Venus (cpVenus) and further mutating the Pi binding domain to generate a series of biosensors, cpFLIPPi with an affinity range (80  $\mu\text{M}$  to 11 mM) suitable for use in plants. To further increase the robustness of cpFLIPPi measurements, Banerjee *et al.* (2016) created cpFLIPPi-Null, which is insensitive to Pi and therefore serves as an important control for nonspecific changes in FRET or fluorescence. Recently, these sensors were used to generate a high resolution map of cytosolic Pi distribution in *Arabidopsis* roots, which revealed that cytosolic Pi levels vary across root development zones but were consistent across cell and tissue types within one zone (Sahu *et al.*, 2020).

Here, we used *B. distachyon* plants expressing cpFLIPPi sensors to monitor the relative Pi levels in the cytosol and plastids of individual cells within a mycorrhizal root and responses to external Pi application.

## Materials and Methods

### Plant material and growth conditions

*Brachypodium distachyon* (line Bd21-3) was used in these experiments. *B. distachyon* seed sterilization and germination were

described previously (Hong *et al.*, 2012). Surface sterilization of *Diversispora epigaea* spores (formerly *Glomus versiforme*) and *Gigaspora gigantea* spores followed protocols described in Liu *et al.* (2004). Two growth systems were used in this study. In the first system, *B. distachyon* plants were grown in 20-cm-long plastic cones filled with a sand-gravel mix of sterile play sand : filter sand : gravel in a 2 : 2 : 1 ratio as previously described (Floss *et al.*, 2017). Plants were inoculated with 100 *D. epigaea* spores or 50 *Gigaspora gigantea* spores placed in the substrate 7 cm below the top of the cones.

Plants were grown in a growth chamber with a 12 h : 12 h, 24°C : 22°C, light : dark cycle. Plants were maintained with deionized water and fertilized once per week with 10 ml of  $\frac{1}{4}$  Hoagland's solution containing 20  $\mu\text{M}$  potassium phosphate. One day prior to imaging, the plants received 10 ml of  $\frac{1}{4}$  Hoagland's solution supplemented with 2  $\mu\text{M}$  potassium phosphate. For experiments involving a high Pi treatment, the plants received 10 ml  $\frac{1}{4}$  Hoagland's solution containing 200  $\mu\text{M}$  Pi at time zero, and were then imaged 0.5, 1, 2 or 18 h later. We chose 200  $\mu\text{M}$  Pi based on results of a pilot experiment (data not shown).

The second growth system was adapted from Giovannetti *et al.* (1993) with modifications. A 10-d-old *B. distachyon* plant and two *Gigaspora gigantea* spores were sandwiched between two cellulose membranes (HAWP09000; Millipore). The spores were placed on each side of the root. Membranes containing the seedlings and spores were planted vertically in the earlier-mentioned sand : gravel mix in an 11 cm diameter pot and grown in the growth chamber in the conditions described for growth system 1.

Roots were used for imaging or assays 4 wk after being transplanted to cones or pots.

### Plasmid generation

All vectors were generated using the multi-site gateway cloning system (Invitrogen). The *BdPT7* (1171 bp upstream of *Bradi2g45520*) and *ZmUbi1* promoters were amplified from *B. distachyon* genomic DNA and the vector pHb7GW-I-WG-UBIL (Karimi *et al.*, 2007; VIB, Ghent, Belgium) respectively, using primers flanked by *attB4L* and *attB1R* recombination sites (Table S1). To create *pDONRp4p1r* vectors containing either the *BdPT7* promoter or the *ZmUbi1* promoter, PCR fragments were recombined into *pDONRp4p1r* using BP recombinase (Invitrogen). *cpFLIPPi-5.3m* (Pi Sensor), *cpFLIPPi-Null* (Control Sensor), *eCFP* and *cpVenus* coding sequences with or without a chloroplast transit peptide (*AtRbcS*), were excised from original vectors, *cpFLIPPi-5.3m*, *cpFLIPPi-Null*, *eCFP* and *cpVenus* (Mukherjee *et al.*, 2015; Banerjee *et al.*, 2016), using *XbaI* and *HindIII* restriction enzymes, respectively. To generate gateway-compatible *pENTR1-2* clones, digested DNA fragments were ligated into an *XbaI*-*HindIII*-digested *pENTR221* vector containing a multiple cloning site from *pUC19*. A *pENTR2-3* plasmid containing the *CaMV35S* terminator was cloned previously (Ivanov & Harrison, 2014). To generate binary vectors for transformation, different combinations of four vectors (*pDONRp4p1r*

containing the *BdPT7* promoter or the *ZmUbi1* promoter; *pENTR1-2* containing one of the four coding sequences; *pENTR2-3 CaMV35S* terminator; and the destination vector *pHb7m34GW* (Karimi *et al.*, 2005)) were assembled using LR recombinase. All constructs were confirmed by Sanger sequencing.

### Generation of *Brachypodium distachyon* transformants

Constructs with *cpFLIPPi-5.3m*, *cpFLIPPi-Null*, *CFP* and *cpVenus* targeted to the cytosol or the plastid expressed from either the *BdPT7* or *ZmUbi1* promoters, were introduced into *B. distachyon* (accession no. Bd21-3) via *Agrobacterium tumefaciens*-mediated transformation (Bragg *et al.*, 2015). Hygromycin was used to select transformed calli. Primary transformants were evaluated for the presence of the appropriate fluorescent signal and genotyped to confirm the presence of the constructs. Multiple independent transgenic lines for each construct were obtained, and 3–4 lines of T2 and T3 generations with equivalent fluorescent intensity were used in the experiments (Table S2). The transgenic lines showed normal growth, and root system development was typical for our experimental conditions. Arbuscule development and infection unit appearance were wild-type in appearance as illustrated in several wheat-germ agglutinin (WGA)-stained images presented in the figures. Unfortunately, transformation failed for *ZmUbi1::cpVenus* and the plastid-targeted sensors expressed from the *ZmUbi1* promoter. In previous studies, the plastid location of these sensor constructs has been validated (Mukherjee *et al.*, 2015). Here, transgenic lines with plastid-targeted sensors expressed from the *BdPT7* promoter showed the expected discrete location and morphology associated with plastids (Supporting Information Fig. S1).

### Radionuclide $^{32}\text{P}$ uptake assay

*Brachypodium distachyon* plants grown between cellulose membranes were used in this assay. Radionuclide  $^{32}\text{P}$  in the form of orthophosphoric acid in water was used (PerkinElmer, Waltham, MA, USA). The  $\frac{1}{4}$  Hoagland's medium containing  $0.01 \mu\text{Ci H}_3[^{32}\text{P}]\text{O}_4$  and 1% agar (Sigma) was freshly made immediately before the experiment and pipetted in  $10 \mu\text{l}$  droplets that were allowed to solidify. The membrane sandwich was opened and one of the membranes was removed. The mycorrhizal roots colonized with *Gigaspora gigantea* were gently rinsed to remove sand particles. Colonized root regions and their connecting fungal hyphae were screened using an Olympus SZX-12 Stereomicroscope to identify hyphae and to track their connections to roots. Infected root zones were readily identified by their density and color. Sites at which to apply the Pi-containing agar blocks were chosen and marked. To allow calculations of the distance between the root and  $^{32}\text{P}$  agar block sites, photographs with distance scales were taken and marked sites were labeled. The  $10 \mu\text{l}$   $^{32}\text{P}$  agar blocks were then placed over the fungal hyphae at the marked sites. The root system on the membrane was enclosed in a 20 cm Petri dish (leaves were outside) and sprayed with  $\frac{1}{4}$  Hoagland's solution without Pi to maintain a moist environment. The plates were incubated in dark for either 0.5, 1, 6 or 18 h.

Following incubation, roots, that were either colonized or not, within a 5 mm radius of the agar block were collected in *c.* 5 mm pieces for scintillation counting and their locations were marked on the photographs. Root samples were immediately dried with paper towels and transferred into scintillation vials filled with 3 ml of Ecoscint H scintillation fluid (National Diagnostics, Atlanta, GA, USA). Each vial was counted three times for 1 min per count (LSC LS6500 scintillation counter; Beckman, Brea, CA, USA) and a mean count value was used for statistical analysis.

To test the rate of  $^{32}\text{P}$  diffusion through the membrane, a  $10 \mu\text{l}$   $^{32}\text{P}$  agar block was placed onto a blank piece of membrane and incubated for 18 h. The membrane was sampled at distances of 0, 4 and 8 mm from the agar block and analyzed by scintillation counting.

For experiments involving a Benomyl pre-treatment, 1 ml of  $100 \mu\text{g} \mu\text{l}^{-1}$  methyl 1-(butylcarbamoyl)-2-benzimidazolecarbamate (Benomyl; Millipore Sigma, Bedford, MA, USA) was applied to the mycorrhizal root system 1 d before the  $^{32}\text{P}$  tracing experiment.

### Pi imaging and image analysis

The preparation of roots for Pi imaging differed slightly for the two growth systems. For growth system 1, the plants were removed from the cones and the roots were placed in a 20 cm Petri dish and rinsed gently with running deionized water to remove the sand. They were then immersed in  $\frac{1}{4}$  Hoagland's solutions with a designated Pi concentration of either  $2 \mu\text{M}$  Pi or  $200 \mu\text{M}$  Pi in the Petri dish. Using a stereomicroscope, a colonized root region was located and moved onto a microscope slide ( $75 \text{ mm} \times 25 \text{ mm}$ ) and covered with a coverslip ( $20 \text{ mm} \times 20 \text{ mm}$ ) to keep it static and flat during imaging. The rest of the root remained attached and was gathered around the edge of the slide and frequently sprayed with the specified Hoagland's solution to keep it moist. The shoot remained attached.

For plants in growth system 2, the cellulose membrane sandwich was opened, and colonized root regions were located and marked using the stereomicroscope. The membrane containing the plant was then transferred onto a glass slide ( $75 \text{ mm} \times 25 \text{ mm}$ ) with the marked region of interest at the center of the slide. A coverslip ( $20 \text{ mm} \times 20 \text{ mm}$ ) was placed on top of the region of interest. During imaging, the membrane was kept wet by spraying with the specified Hoagland solution. To find the same cells before and after local Pi feeding, imaged sites were recorded. The mounting process for both growth systems took *c.* 5 min and it was counted as part of the incubation time when local Pi feeding was used.

Roots were imaged with a Leica TCS SP5 Confocal Microscope equipped with an Argon laser and two HyD detectors using settings described in Table S3. The same optimized confocal settings were used for all experiments (Table S3). Donor (enhanced cyan fluorescent protein (eCFP)) bleedthrough and acceptor (*cpVenus*) cross-excitation were measured to calculate sensitized FRET (Rincón-Zachary *et al.*, 2010; Banerjee *et al.*, 2016). For each experiment this requires imaging of individual plants expressing the Pi sensor, the Pi-insensitive control sensor, and the

two single fluorophore controls (*B. distachyon* roots expressing eCFP and cpVenus separately). As we lacked plants expressing *ZmUbi1::cpVenus*, plants expressing *BdPT7::cpVenus* were used as a control. Any background autofluorescence, including that arising from the AM fungi (an example shown in Fig. S2) is accounted for in the sensitized FRET calculation and through the use of the Pi-insensitive control sensor (Table S4).

Image processing and analysis were as previously described (Mukherjee *et al.*, 2015; Banerjee *et al.*, 2016), using a customized macro in Fiji (IMAGEJ) (script in Methods S1). Sensitized FRET (FRET : eCFP) ratios were calculated as described in Mukherjee *et al.* (2015) and shown in the figures as FRET ratio (Table S4 provides the equation and an example of the calculations). The calculated sensitized FRET was displayed as pseudo-color images generated using Fiji (script in Methods S2). Z-stacks were also generated in Fiji using Z project. As reported previously, assay linearity was confirmed for each experiment (Table S4; Banerjee *et al.*, 2016). If changes in FRET ratios were detected for both Pi and control sensors, delta FRET ratios were calculated as reported previously (Banerjee *et al.*, 2016). A delta FRET ratio for the control sensor indicates a non-Pi-specific effect, whereas a delta FRET ratio for the Pi sensor reflects the combination of both specific and nonspecific effects, and the Pi-specific effect is the difference between the two.

#### Visualization of arbuscules with WGA-Alexa Fluor 488 staining

After Pi imaging, roots were immediately stained *in situ* with wheat-germ agglutinin-Alexa Fluor 488 (WGA-AF488; Invitrogen) to detect arbuscules. Roots were immobilized under a thin layer of 1% agar (Sigma) between the coverslip and the glass slides by pipetting 0.5 ml of molten agar into the gap (Brown & Lemmon, 1995; Blancaflor *et al.*, 2001). The immobilized root was then excised and separated from the plant. Root segments were fixed and stained according to Hong *et al.* (2012) with the following modifications. Roots were fixed in 50% ethanol for 3 d and then cleared in 20% (w/v) potassium hydroxide for 5 d. Roots were stained with 0.2  $\mu\text{g ml}^{-1}$  WGA for 2 d at 4°C. FRET images were used as references to locate arbuscules. WGA-AF488 was excited with an argon laser (488 nm) and emission was collected from 500 to 550 nm. Then, 10–20 Z-stack images (slice distance: 1  $\mu\text{m}$ ) were collected to visualize arbuscules.

#### Statistical analyses

All experiments were performed using at least six biological replicates except for the  $^{32}\text{P}$  uptake experiment, which had at least three biological replicates. All experiments were repeated two to three times. All statistical analyses were performed using R. The normality of every data set was tested using the Shapiro–Wilk test. Pairwise comparisons were made using two-tailed Student's *t*-tests for normally distributed data sets; otherwise, nonparametric Mann–Whitney *U*-tests were used. For multiple comparisons, if a data set was normally distributed, ANOVA followed by a

Tukey's HSD *post hoc* test was performed on the raw data. Otherwise, a Kruskal–Wallis test followed by a two-tailed Dunn's *post hoc* test was performed.

## Results

### *Brachypodium distachyon* transgenic lines expressing Pi sensors for live imaging of Pi in the cytosol and plastids

To image Pi in the cytosol of *B. distachyon* mycorrhizal root cells, we generated transgenic lines expressing a second-generation Pi sensor (cpFLIPPI-5.3m), single fluorescent protein controls, and a Pi-insensitive control sensor (cpFLIPPI-Null), from either the constitutive *ZmUbi1* promoter or a mycorrhiza-inducible, cell-type specific *BdPT7* promoter (Table S2). *BdPT7* is the ortholog of *Medicago truncatula* PT4 and *Orzya sativa* PT11 (Harrison *et al.*, 2002; Paszkowski *et al.*, 2002; Hong *et al.*, 2012). Similarly, to image Pi in plastids of mycorrhizal root cells, transgenic lines expressing plastid-targeted versions of the sensors (cpFLIPPI-5.3m and cpFLIPPI-Null) (Mukherjee *et al.*, 2015; Banerjee *et al.*, 2016) under control of the *BdPT7* promoter were generated (Table S2). Despite multiple attempts, we failed to regenerate lines constitutively expressing plastid-targeted sensors. This may be a consequence of the tissue culture-based transformation approach because constitutively expressed, plastid-targeted sensors lines have been generated in *Arabidopsis* (Mukherjee *et al.*, 2015).

### Cytosolic Pi levels are higher in *Diversispora epigaea*-colonized cells than in adjacent epidermal cells

We first wanted to ask whether cytosolic Pi levels differ between colonized cells and noncolonized cells in a mycorrhizal root. To make this comparison, *B. distachyon* lines constitutively expressing the Pi sensor (cpFLIPPI-5.3m) and Pi-insensitive control sensor (cpFLIPPI-Null) were inoculated with *D. epigaea* and then imaged 4 wk post-inoculation. Emission from direct excitation of cpVenus indicated that sensor abundance in these cell types was similar (Fig. 1a). Ratiometric imaging (FRET : eCFP), referred to as FRET ratio hereafter, was then used to assess relative Pi levels (Mukherjee *et al.*, 2015; Banerjee *et al.*, 2016). The *B. distachyon* roots that we imaged here had only one layer of cortical cells, so for this initial comparison, we compared colonized cells containing fully developed, mature arbuscules with adjacent, noncolonized epidermal cells. As shown in the representative pseudo-color images and by quantitative analysis, Pi-dependent FRET ratios were lower, indicating higher Pi levels, in colonized cells than in epidermal cells (Fig. 1a,b). In contrast, FRET ratios for the Pi-insensitive control sensor did not differ between these two cell types, indicating that differences detected with the Pi sensor can be attributed to differences in relative cytosolic Pi levels. These findings were further confirmed in a parallel experiment, which included colonized roots and also noncolonized roots (from mock-inoculated plants) (Fig. S3). In colonized roots, the Pi content of the colonized cortical cells was higher than that of the epidermal cells, while in noncolonized roots, the

Pi content of cortical and epidermal cells did not differ from each other (Fig. S3).

Hong *et al.* (2012) showed that *B. distachyon* shoot P content was higher when associated with *D. epigaea* than with *Gigaspora gigantea*. We therefore investigated the relative cytosolic Pi levels in roots colonized with these two AM fungi. As shown in Fig. 1 (c), FRET ratios from the Pi sensor were similar in epidermal cells in the two mycorrhizal root systems. In contrast, the Pi sensor showed a lower ratio in cells colonized by *D. epigaea* than cells colonized by *Gigaspora gigantea* (Fig. 1d). FRET ratios from the control sensor did not differ in either comparison. Consequently, we conclude that cytosolic Pi levels are higher in root cells colonized by *D. epigaea* than *Gigaspora gigantea*, which aligns with earlier observations of shoot P content.

Next, we sought to determine whether Pi levels differ between cells containing distinct fungal structures. We imaged cells with intracellular hyphae (IH), cells in which arbuscules filled the cell (mature arbuscules,  $A_M$ ) and cells with arbuscules that had degenerated to clumps (collapsed arbuscules,  $A_C$ ) (Fig. 1e). Regions of interest (ROIs) were applied to cytosolic regions associated with the hypha, arbuscule branches, or arbuscule clumps, respectively. Quantitative analyses showed that FRET ratios from the Pi sensor did not differ between these cells. This result was unexpected as we anticipated that the  $A_M$  cells would have the highest Pi levels. However, if differences between these cells exist, they are below the limits of detection with this Pi sensor.

### Plastidic Pi levels are highest in cells at the growing front of an infection unit

Given that development and functioning of AM symbiosis requires several products of plastid metabolism (MacLean *et al.*, 2017), we first asked whether plastids within a single colonized cell show any variation in Pi levels. Transgenic lines with plastid-localized Pi and control sensors expressed from the BdPT7 promoter were colonized with *D. epigaea* and then FRET ratios were quantified in plastids in 10 randomly selected cells that contained mature arbuscules. Comparisons of FRET ratios in six ROIs across three optical sections in each of 10 cells indicated that plastids within a single cell have the same relative Pi level (Fig. S4).

Next, we imaged plastids in cells across an entire infection unit. This enabled a systematic comparison of plastids in cells containing arbuscules at different developmental stages. For ease of comparison, the infection units were divided into three regions: the region proximal to the growing hyphal front (1), the middle region (2), and the region distal to the hyphal front (3) (Fig. 2a). Each region covered 3–5 longitudinally-positioned cells. The pseudo-color images (Fig. 2b) from the Pi sensor suggested that within the region 1, FRET ratios in cells at the growing hyphal front (region  $1_a$  in Fig. 2a) were lower than those a few cells behind (region  $1_b$  in Fig. 2a) and potentially lower than those in region 2. Quantitative analyses of roots expressing the Pi sensor revealed that FRET ratios in cells in position  $1_a$  were lower than those in  $1_b$  and lower than cells in region 2 (Fig. 2c). However, roots expressing the control sensor also showed differences in FRET ratios between cells in

these regions indicating that Pi sensor responses cannot be attributed solely to differences in Pi levels. To address this issue, we compared delta FRET ratios for both sensors in cells at position  $1_b$  vs  $1_a$  and for cells at position  $1_b$  vs cells in region 2 (Fig. 2d). For cells in  $1_b$  vs  $1_a$ , the delta values for the Pi sensor were larger than those of the control sensor, and the difference was statistically significant. Therefore, there is a statistically significant difference in Pi in the plastids of cells in region  $1_b$  vs  $1_a$  with higher Pi levels in the plastids of cells in  $1_a$ . In contrast, differences were not significant for cell types in the middle region vs cells in  $1_b$  (Fig. 2d).

Arbuscules in cells at the growing front of the infection unit (position  $1_a$ ) are typically in the earliest stages of development, while those in position  $1_b$  are typically more advanced in their development. To overlay the developmental status of the arbuscules with Pi imaging, arbuscules were visualized by staining *in situ* with WGA-AF488 (Fig. 2b). There were differences in the arbuscules in position  $1_a$  vs  $1_b$  (Fig. 2b). Cells at position  $1_a$ , contained arbuscules with many thick branches, i.e. developing arbuscules, while cells at position  $1_b$ , had arbuscules that contained more thin branches, i.e. in their late stages of development (Fig. 2b). This suggests that in colonized cells, plastidic Pi levels decrease as the arbuscules develop, likely as a result of changes in their metabolic activity.

Plastid morphology varies in colonized root cells; the plastids are stromulated in cells with developing and mature arbuscules, while they are typically lens-shaped in cells in which arbuscules have collapsed (Ivanov & Harrison, 2014). We hypothesized that relative plastidic Pi levels would vary between the two shapes of plastids. In region 3, cells with lens-shaped plastids (L) can be found directly adjacent to cells with stromulated plastids (S) which allows comparisons of the effects of shape without any confounding effects of longitudinal position (Figs 2b, S5). Quantitative analysis showed no difference in plastidic Pi levels in these two cell types (Fig. 2e), indicating the relative Pi levels in plastids of different shapes remain the same, at least within the detection range of this sensor. Furthermore, the relative Pi levels of plastids in cells in region 2 did not differ from those in cells in region 3 ( $P=0.34$ ,  $n \geq 29$ , Student's *t*-test).

### Pi application to the root system elicits a transient increase in cytosolic Pi in arbuscule-containing cells

To determine if colonized cells show temporal responses to a Pi increase in the external environment, plants expressing the symbiosis-specific cytosol-localized sensor (*BdPT7::cpFLIPPi-5.3m*) and the respective control sensor (*BdPT7::cpFLIPPi-Null*), each colonized with *D. epigaea* were treated with a single application of  $\frac{1}{4}$  Hoagland's solution containing 200  $\mu$ M Pi. Focusing on cells that contained mature arbuscules, Pi imaging was carried out before external Pi application (0 h) and again after 0.5, 1, 2 and 18 h. FRET ratios for the Pi sensor decreased 0.5 h after Pi application but returned to the pre-treatment levels by 1 h and then remained relatively constant (Fig. 3a,b). In contrast, FRET ratios for the control sensor remained constant during this period. These results indicate a transient increase in cytosolic Pi in colonized cells. This

finding was supported by a similar experiment using plant lines expressing the constitutively expressed Pi sensor. Again, in the colonized cortical cells, FRET ratios for the Pi sensor showed a transient decrease 0.5 h post-Pi application (Fig. 3c). These data indicate a transient increase in cytosolic Pi levels of cells containing arbuscules

following Pi application to the mycorrhizal root. Considering the speed of the response, we speculate that the observed changes result from Pi that was taken up by the root directly.

Using *B. distachyon* lines expressing plastid-targeted sensors, we carried out a similar experiment to monitor plastidic Pi

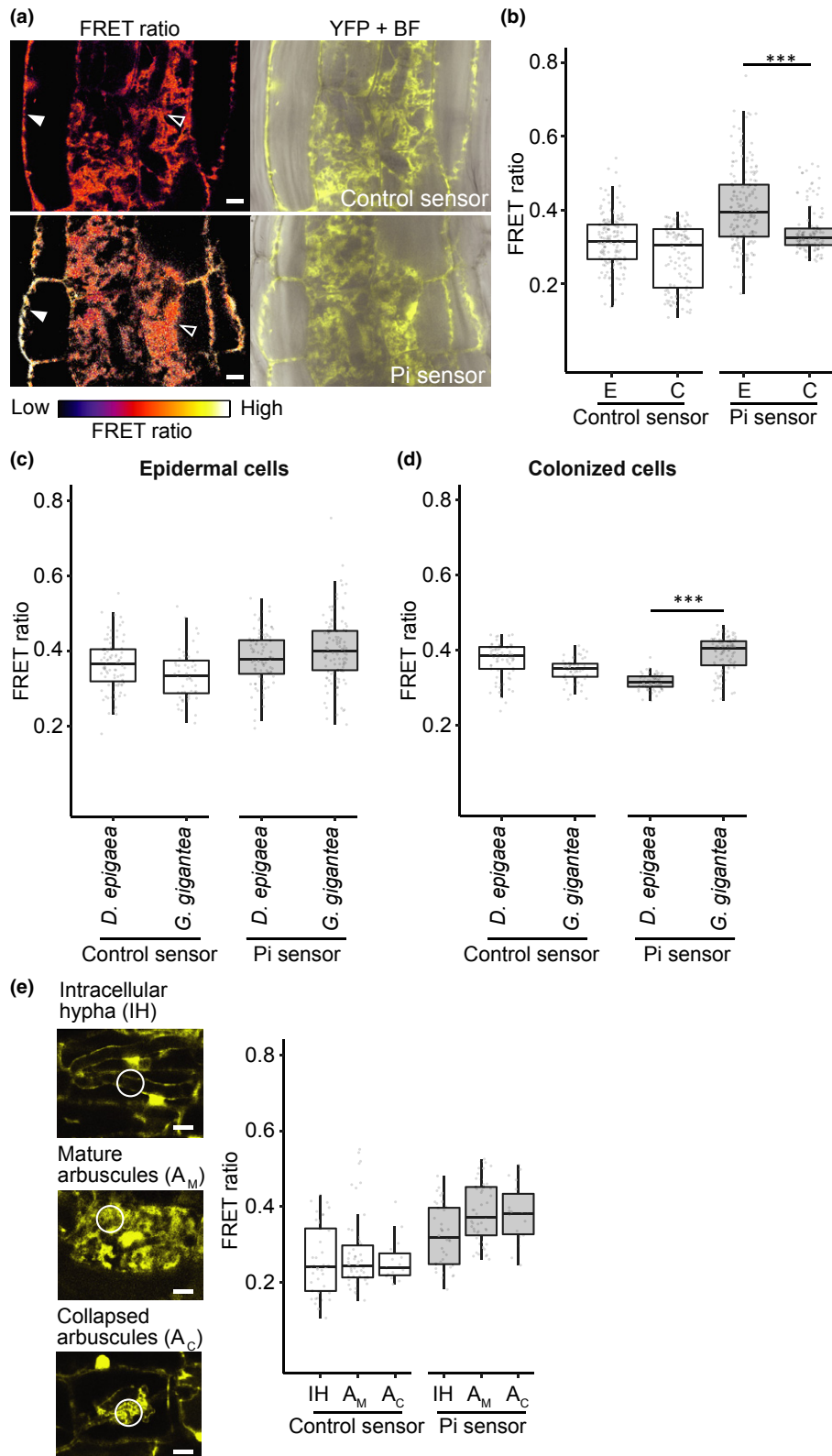


**Fig. 1** Live imaging of cytosolic orthophosphate (Pi) in *Brachypodium distachyon* roots associated with arbuscular mycorrhizal (AM) fungi *Diversispora epigaea* or *Gigaspora gigantea*. (a) Representative pseudo-color images of fluorescence resonance energy transfer (FRET) ratio, and yellow fluorescent protein (YFP) and brightfield (BF) merged images from *B. distachyon* roots expressing a Pi-insensitive control sensor or a Pi sensor. Filled arrowhead, epidermal cells; empty arrowhead, *D. epigaea*-colonized cells. Bar, 10  $\mu\text{m}$ . (b) FRET ratios from roots expressing either the control sensor or the Pi sensor as in (a). E, epidermal cells; C, *D. epigaea*-colonized cells. In roots expressing the Pi sensor, differences between E and C cells are significant (\*\*\*,  $P < 0.001$ , Mann–Whitney  $U$ -tests). (c, d) FRET ratios in epidermal cells (c) and colonized cells (d) of roots colonized with either *D. epigaea* or *Gigaspora gigantea*. Data from roots expressing the control and Pi sensors are shown. For the Pi sensor, differences between *D. epigaea*-colonized cells and *Gigaspora gigantea*-colonized cells are significant (\*\*\*,  $P < 0.001$ , Mann–Whitney  $U$ -tests). (e) Left, Representative cpVenus images of *D. epigaea*-colonized cells showing intracellular hyphae (IH), mature arbuscules ( $A_M$ ) and collapsed arbuscules ( $A_C$ ); circles indicate typical regions of interest (ROIs) chosen for the quantification. Bar, 10  $\mu\text{m}$ . Right, FRET ratios from colonized cells containing either IH,  $A_M$  or  $A_C$  as indicated in the left panel. Significant differences were not observed (Tukey's HSD tests were performed independently for each sensor). The box plots in (b–e) show the lower and upper quartiles, and the minimum and maximum values. The bar in the box plots represents the median. Each gray point in the boxplots represents a measurement from one ROI per cell. Measurements were made on more than 32 cells.

responses. In contrast to the cytosolic Pi sensor, the FRET ratios of the plastid Pi sensor did not change (Fig. 3d), indicating that plastidic Pi levels are not influenced by this external Pi treatment.

### Cytosolic Pi levels and cytosolic Pi response dynamics vary across cell types within a mycorrhizal root

Having observed temporal changes in cytosolic Pi accumulation in cells containing mature arbuscules, we asked how other cells within the mycorrhizal root respond to a high external Pi treatment. Using colonized *B. distachyon* plants with constitutively expressed sensors, five cell types were imaged before and after Pi application: epidermal cells (E), noncolonized cortical cells (N), cells containing IH, cells containing  $A_M$  and cells containing  $A_C$  (Fig. S6). Visualization of responses in individual cell types over time and comparisons of relative Pi levels across cell types are displayed through a heat map (Fig. 4a) as well as graphs that provide details of FRET ratios in cell types and over time (Figs 4b, S7; Table S5). The data are consistent with earlier experiments in that the three colonized cell types did not differ in relative cytosolic Pi levels prior to treatment and, as observed previously,  $A_M$  cells showed a transient decrease in FRET ratios, consistent with an increase in cytosolic Pi, at 0.5 h. Surprisingly, FRET ratios in  $A_C$  cells increased at 0.5 h post-Pi treatment (Figs 4, S7), indicating that relative cytosolic Pi levels decrease transiently in these cells in response to external Pi. The IH cell type did not show a significant response to Pi treatment.

Noncolonized cortical cells have a lower relative cytosolic Pi level than colonized cells and also respond to Pi treatment differently with no significant change at 0.5 h, but Pi levels increase at 1 h post-Pi treatment (Figs 4, S7). Despite this increase, relative Pi levels in this cell type remain much lower than those in  $A_M$  cells. Prior to Pi treatment, epidermal cells have higher cytosolic Pi levels than noncolonized cortical cells, but not as high as colonized cortical cells. The epidermal cell response to Pi treatment is similar in trajectory to that of the  $A_C$  cells in that they show a substantial transient decrease in Pi level 0.5 h post-Pi treatment followed by a slight increase 1 h post-treatment. At 0.5 h post-Pi treatment the epidermal cells showed the lowest Pi level while  $A_M$  cells showed the highest Pi level.

In summary, these data indicate that cells of a mycorrhizal root differ in their relative cytosolic Pi levels and also in the dynamics of their responses to Pi treatment (Figs 4, S7).

### Pi levels in colonized cortical cells increase 18 h after Pi application to *Gigaspora gigantea* extraradical hyphae

Pi sensors provide the means to monitor Pi delivery to the cortical cells via the fungal symbiont; however, such experiments require an experimental setup in which Pi can be applied specifically to the extraradical hyphae (ERH) rather than to the entire mycorrhizal root system. To achieve localized feeding of Pi directly to the ERH, we adapted a membrane sandwich system from Giovannetti *et al.* (1993) and Novero *et al.* (2002) and then evaluated the time frame for symbiotic Pi transfer using radioisotope tracing. Briefly, *B. distachyon* roots and *Gigaspora gigantea* spores were sandwiched between two pieces of cellulose membranes, which were then placed in pots to allow the association to develop (Fig. 5a–d). Membrane sandwiches were then removed from the pots, opened, and small blocks of agar impregnated with  $^{32}\text{P}$  were placed on the ERH. Radioactivity in both colonized and noncolonized regions of the root, within a 5 mm radius of the source, was monitored at 0.5, 1, 6 and 18 h post-application. Statistically significant increases in radioactivity in the colonized root regions were detected at 18 h (Fig. 5e). Measurements from the noncolonized regions indicate that  $^{32}\text{P}$  diffusion across the membrane surface was low (Table S6), therefore supporting the conclusion that colonized regions received  $^{32}\text{P}$  via the fungus. To further confirm that the Pi was transferred by the AM fungus, a Benomyl pretreatment was applied to kill the fungus. At 18 h, colonized root regions (C) had twice the radioactivity compared to the Benomyl-pretreated colonized regions (BC) and also to the noncolonized (NC) and Benomyl-pretreated noncolonized (BNC) regions (Fig. 5f). Together, these results support active transfer of Pi to the roots via the ERH and indicate that statistically significant increases are detectable 18 h following application.

These  $^{32}\text{P}$  tracing experiments provide a time frame for transfer through the hyphae to the root system but lack the cellular resolution needed to determine whether Pi enters the root cytosol. To address this, we repeated the experiment using plants expressing the sensors driven from the BdPT7 promoter (Fig. 5d) and omitting the radiotracer. FRET ratios were measured in individual cells containing mature arbuscules before Pi application and then in the same cells 18 h after local Pi feeding to the ERH. Quantitative analyses showed changes in FRET ratios for the Pi sensor and a smaller change from the control sensor (Fig. 6). Delta FRET ratios indicate an increase in cytosolic Pi levels in

the colonized cells 18 h post-Pi treatment suggesting that Pi is transferred from the arbuscule and can be detected in the root cell within this time frame. In summary, using both radiotracing and Pi biosensors provides a means to monitor Pi transfer through the ERH and delivery to the root cell cytosol.

## Discussion

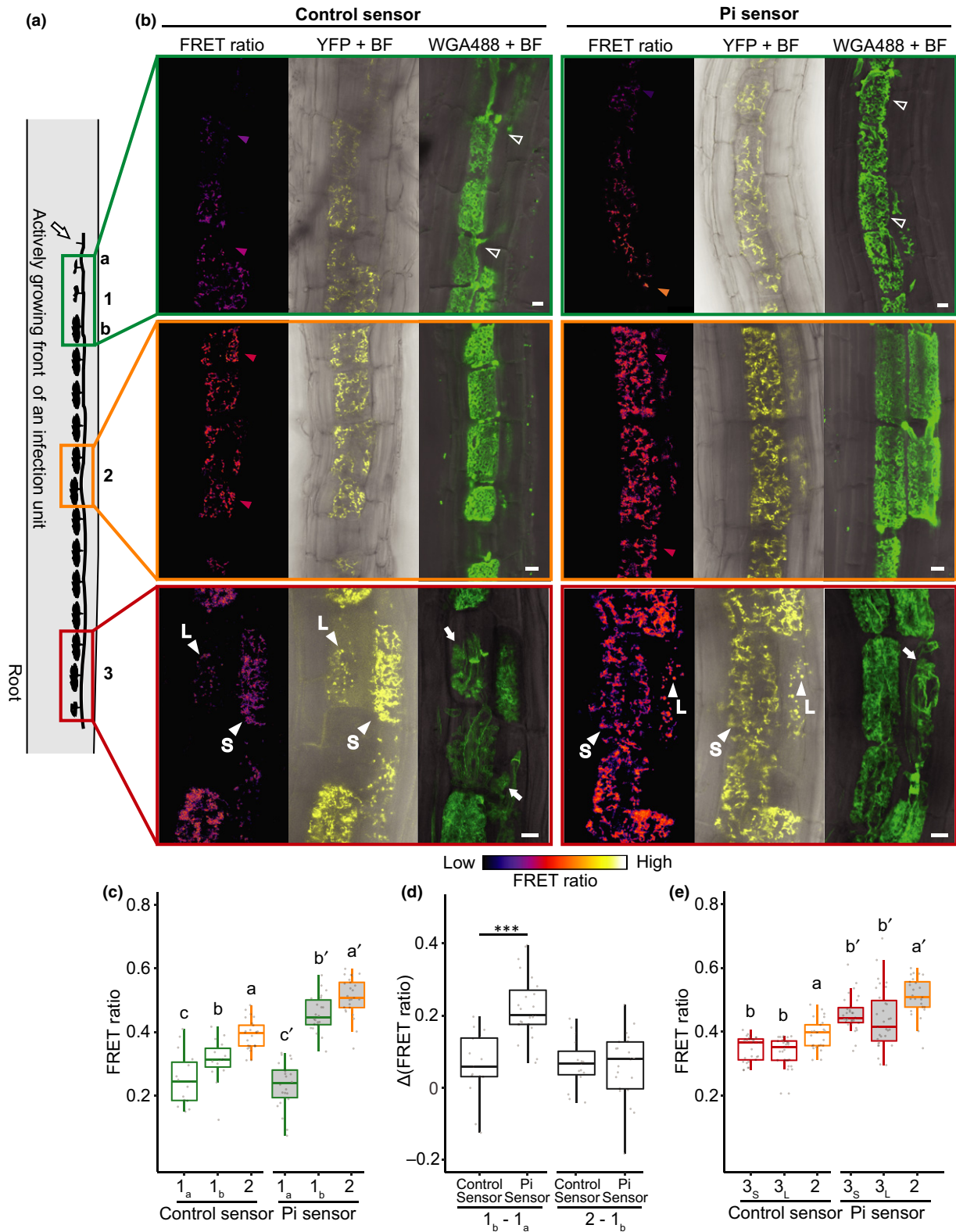
Development of endosymbiosis with AM fungi results in substantial changes in the cellular structure and metabolism of the colonized cortical cells as well as a new pathway for Pi entry to the root. While much research has focused on Pi transporters and their roles in symbiotic Pi transfer, we have little knowledge of how the association affects cellular Pi content. Here, spatiotemporal comparisons of intracellular Pi across cells of a mycorrhizal root showed that steady-state cytosolic Pi levels differ between cell types. Furthermore, cytosolic Pi content varies in response to Pi application to the root and individual cell types differ in the trajectory and dynamics of this response.

Using *B. distachyon*, which was chosen because its roots are thin enough to allow direct imaging of the cortical cell layer, a series of experiments revealed that the cytosolic Pi content of cells with mature arbuscules ( $A_M$  cells) is higher than that of noncolonized cortical cells and also higher than epidermal cells. Colonized cells are unique in that they receive Pi via the arbuscule, with estimated flux rates of  $1.3 \times 10^{-14} \text{ mol mm}^{-2} \text{ s}^{-1}$  (Cox & Tinker, 1976), which may explain their higher cytosolic Pi levels. Somewhat surprisingly, cells containing intracellular hyphae (referred to IH cells) showed relative cytosolic Pi levels similar to that of colonized cells. It is generally assumed that in the intracellular hyphae do not contribute Pi transfer to the plant. However, this assumption is based on the location of the plant mycorrhiza-induced Pi transporters on the periarbuscular membrane (Harrison *et al.*, 2002; Kobae & Hata, 2010). The possibility that Pi transfer occurs across other fungal–plant interfaces, with uptake mediated by constitutively expressed Pi transporters, has not been investigated. Alternatively, intracellular hyphal continuity between IH cells and adjacent arbuscule-containing cells within the same cell file might influence Pi distribution between these cells.

Following Pi application to the root system, colonized and noncolonized cells differed in the dynamics and trajectory of their cytosolic Pi response. This suggests that these cell types differ in some, or all, of the typical factors that influence cytosolic Pi levels, including Pi transport, vacuolar sequestration, cellular structure and metabolic transformations (Plaxton & Tran, 2011; Versaw & Garcia, 2017; Dissanayaka *et al.*, 2021). That  $A_M$  cells and noncolonized cells differ in the latter two factors is well established. For example, in  $A_M$  cells the vacuole volume decreases as the arbuscule occupies space within the cell but the tonoplast surface area increases (Cox & Tinker, 1976; Bonfante-Fasolo, 1984). These alterations could influence Pi transport across the tonoplast as well as the potential Pi buffering capacity of the vacuole, which serves as the main Pi store in plant cells. In Arabidopsis root cells, vacuole Pi loading was largely independent of vacuole size, but vacuolar Pi transport influenced cytosolic Pi levels differentially across the transition, elongation and mature zones (Sahu *et al.*, 2020). Currently, we lack information about Pi transport activities on the tonoplast of  $A_M$  cells, but it is possible that this parameter differs between  $A_M$  and noncolonized cortical and epidermal cells. Cellular metabolism, including fatty acid biosynthesis and membrane production, in  $A_M$  cells differs from that of noncolonized cells and may also contribute to differing cytosolic Pi responses (Bravo *et al.*, 2017; Keymer *et al.*, 2017).

The contrasting Pi response dynamics in the  $A_M$  cells vs epidermal cells could also arise from differences in Pi transport and Pi content. It is well documented that mycorrhizal roots downregulate Pi uptake transporters in the root epidermis which may partly explain this low cytosolic Pi content relative to that of  $A_M$  cells (Paszowski *et al.*, 2002; Liu *et al.*, 2008, 2016) (Fig. 4). These epidermal cells may be Pi-starved relative to  $A_M$  cells, a physiological difference that could also influence Pi response dynamics. The decrease in cytosolic Pi levels in the epidermal cells at 30 min post-Pi application may reflect Pi transfer to the vacuole and/or incorporation into adenosine triphosphate (ATP) and other organic compounds (Arisz *et al.*, 2009; Dissanayaka *et al.*, 2021), both of which are known to occur within minutes of Pi uptake into plant cells (Sahu *et al.*, 2020). Pi transfer to the vacuole occurs even more rapidly in Pi-deprived cells (F. Liu *et al.*, 2016; T.-Y. Liu *et al.*,

**Fig. 2** Plastidic fluorescence resonance energy transfer (FRET) ratios across an infection unit in a *Brachypodium distachyon*/*Diversispora epigaea* mycorrhizal root. (a) A schematic diagram of an infection unit in a colonized root. Three regions of the infection unit were chosen for quantification: region 1 is proximal to the actively growing front of an infection unit (green box) and within region 1, the two ends are labeled a and b; region 2 in the middle of an infection unit (orange box) and region 3 is distal to the actively growing front of an infection unit (red box). (b) Representative pseudo-color images of FRET ratios, yellow fluorescent protein (YFP) and brightfield (BF) merged images and wheat germ agglutinin-Alexa Fluor 488 (WGA-AF488) and BF merged images from roots expressing the control sensor and orthophosphate (Pi) sensor. Images outlined in the green, orange and red boxes were chosen from the regions as indicated in (a), respectively. Filled arrowheads with colors are indicative of the FRET ratio in that cell; empty arrowheads indicate arbuscules; filled white arrowheads indicate stromulated plastids (S) or lens-shaped plastids (L); filled white arrows indicate cells containing collapsed arbuscules. Bar, 10  $\mu\text{m}$ . (c) Plastidic FRET ratios from cells in region 1 (two sub-regions are shown, 1<sub>a</sub> and 1<sub>b</sub>, green boxes) and region 2 (2, orange boxes) as indicated in (a). An ANOVA was performed separately for each sensor. Significant differences ( $P < 0.05$ , Tukey's HSD tests) are indicated by a, b, c, and a', b', c', respectively. (d) FRET ratio differences ( $\Delta\text{FRET}$  ratio) between cells in regions 1 and 2 as indicated in (a). The  $\Delta\text{FRET}$  ratio was calculated using the data in (c). For the 1<sub>a</sub> and 1<sub>b</sub> comparison, the Pi sensor shows a larger  $\Delta\text{FRET}$  ratio value than the control sensor and the difference is significant (\*\*\*,  $P < 0.001$ , Student's *t*-tests). (e) FRET ratios from stromulated and lens-shaped plastids in cells in region 3 (red box) and with stromulated plastids in region 2 (orange box) as indicated in (a). S, stromulated plastids from the distal region; L, lens-shaped plastids from the distal region; 2, stromulated plastids in the middle region (individual cells contain either stromulated plastids or lens-shaped plastids). An ANOVA was performed separately for each sensor. Significant differences from Tukey's HSD tests ( $P < 0.05$ ) are denoted by a, b, and a', b', respectively. The box plots in (c–e) show the lower and upper quartiles, and the minimum and maximum values. The bar in the box represents the median. Each gray point in the boxplots represents a measurement from one region of interest (ROI) per cell. Measurements were made on at least 22 cells.



2016; Sahu *et al.*, 2020; Dissanayaka *et al.*, 2021), so the 30 min time point in our experiments was likely too slow to detect any initial increase in cytosolic Pi in the epidermal cells. Our measurements reflect steady-state levels as the cells reset their Pi

homeostasis and, as noted earlier, differences in cell structure and metabolism influence the steady-state cytosolic Pi levels.

Also notable, cells with collapsed arbuscules (referred to as A<sub>C</sub> cells) showed a cytosolic Pi response similar in trajectory to the

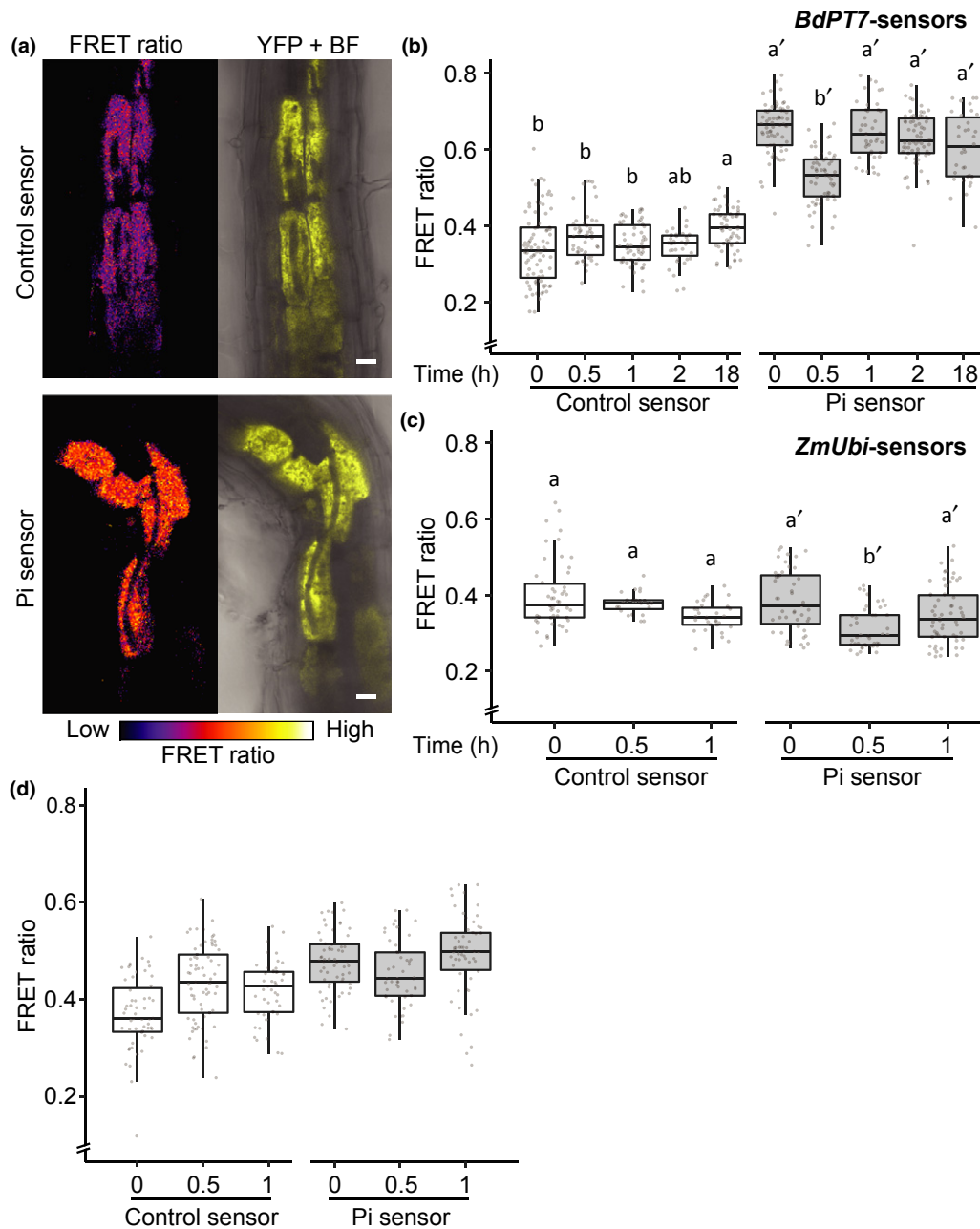


**Fig. 3** Temporal changes of the cytosolic and plastidic fluorescence resonance energy transfer (FRET) ratios following orthophosphate (Pi) application to a *Brachypodium distachyon*/*Diversispora epigaea* mycorrhizal root system. (a) Representative pseudo-color images of cytosolic FRET ratios and yellow fluorescent protein (YFP) and brightfield (BF) merged images from roots expressing control or Pi sensors in the cytosol exclusively in colonized cells (sensors expressed from the *BdPT7* promoter). Bar, 10  $\mu$ m. (b, c) Cytosolic FRET ratios from colonized cells expressing sensors either specifically in colonized cells (b, *BdPT7* promoter) or constitutively in all the root cells (c, *ZmUbi* promoter) before (0 h) and 0.5, 1, 2, and 18 h after high Pi application. ANOVA (b) and Kruskal–Wallis (c) tests were performed for each sensor. Different letters and letters with primes denote significant differences ( $P < 0.05$ ) from Tukey's HSD *post hoc* tests in (b) and Dunn's *post hoc* tests in (c). (d) Plastidic FRET ratios from colonized cells expressing plastid-targeted sensors before (0 h) and 0.5 and 1 h after high Pi application. ANOVA was performed independently for each sensor. Significant differences were not observed. In (b–d), statistical analyses were performed for each sensor. The box plots show the lower and upper quartiles, and the minimum and maximum values. The bar in the box represents the median. Each gray point in the boxplots represents a measurement from one region of interest (ROI) per cell. Measurements were made on more than 45 cells.

noncolonized cells with a transient decrease in cytosolic Pi and a subsequent increase at 1 h. Perhaps this reflects the cellular transition of  $A_C$  cells back to their noncolonized state, and the reinstatement of the large central vacuole which occurs once the arbuscule has collapsed (Bonfante-Fasolo, 1984).

Pi efflux from cells may also influence cytosolic Pi content. In *Arabidopsis*, tracer experiments reveal that Pi distribution through the root and even to the shoot, can be detected within 30 min of Pi application (Kanno *et al.*, 2016) suggesting Pi uptake and efflux activities operating within this time frame.

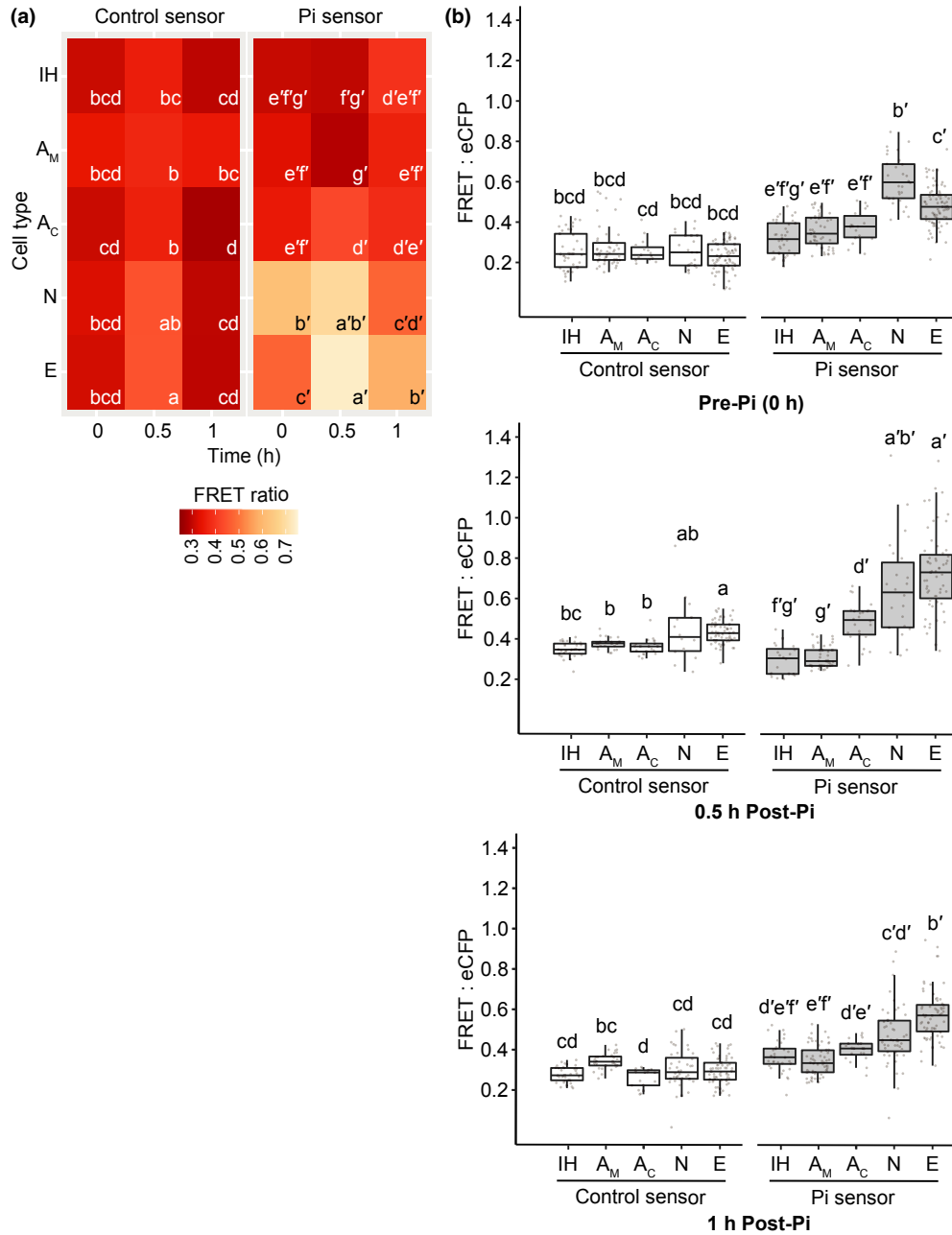


**Fig. 4** Temporal changes in cytosolic fluorescence resonance energy transfer (FRET) ratios in five different cell types following orthophosphate (Pi) application to *Brachypodium distachyon*/*Diversispora epigaea* mycorrhizal roots. (a) A heat map showing cytosolic FRET ratios from five root cell types before Pi application (0 h) and at 0.5 and 1 h post-Pi application. IH, cells with intracellular hyphae; A<sub>M</sub>, cells with mature arbuscules; A<sub>C</sub>, cells with collapsed arbuscules; N, noncolonized cortical cells; E, epidermal cells. A Kruskal–Wallis test was performed separately for each sensor. Different letters and letters with primes indicate significant differences between different combinations of cell type and time for each sensor after Dunn's *post hoc* tests ( $P < 0.05$ ,  $n \geq 20$ ). (b) Box plots showing FRET ratios across five cells types (IH, A<sub>M</sub>, A<sub>C</sub>, N, and E) at three time points 0 h (before Pi application), 0.5 and 1 h post-Pi application. These box plots show the data presented in the heat map in (a). The box plots show the lower and upper quartiles, and the minimum and maximum values. The bar in the box represents the median. Each gray point in the boxplots represents a measurement from one region of interest (ROI) per cell. Measurements were made on more than 19 cells.

Currently, we have little knowledge of Pi efflux systems in cells in a mycorrhizal root. While mechanistic explanations require further experimentation, our measurements reveal considerable differences in relative cytosolic Pi content and response dynamics across mycorrhizal root cell types.

At the subcellular level, the relative Pi content of the plastids was uniform across cells and in response to changes in external Pi. However, we could detect a short gradient in the plastidic Pi levels in cells at the active growing front of an infection unit, with a higher Pi level in cells with younger (less branched) arbuscules

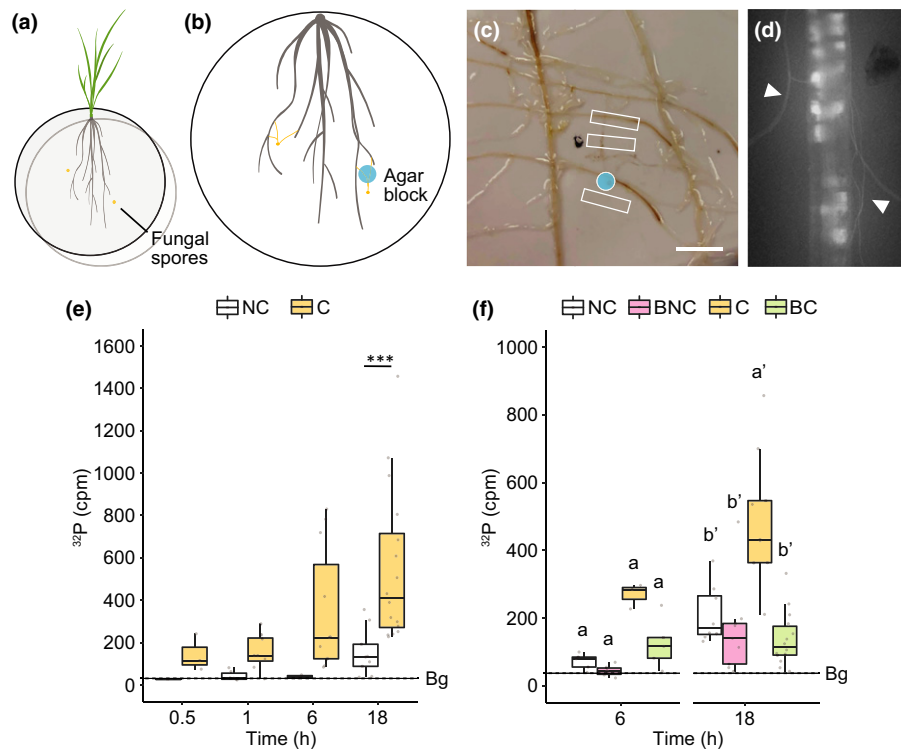


**Fig. 5** Tracing  $^{32}\text{P}$  to *Brachypodium distachyon* roots by *Gigaspora gigantea*. (a, b) Schematic diagrams of the experimental system used for local application of  $^{32}\text{P}$  to *Gigaspora gigantea* extraradical hyphae. (a) Depicts a *B. distachyon* plant and two *Gigaspora gigantea* spores (yellow dots) between two cellulose membranes. (b) An agar block (blue circle) containing  $^{32}\text{P}$  was placed over the extraradical hyphae (yellow lines). (c) An example of Pi-containing agar placement (blue circle) over the extraradical hyphae and the root regions collected for radioactivity counting (white boxes). Bar, 5 mm. (d) A representative stereo microscope image showing fluorescence from the cytosolic Pi sensor and the positions at which the extraradical hyphae attach to the root (arrowheads). (e) Counts per minute (cpm) from noncolonized root regions (NC, white bars) and colonized root regions (C, yellow bars) at 0.5, 1, 6, and 18 h after  $^{32}\text{P}$  application. Pairwise Mann–Whitney tests were performed separately for each time point, and significant differences are indicated (\*\*\*,  $P < 0.001$ ). (f) Counts per minute (cpm) root regions collected from Benomyl pre-treated mycorrhizal root systems 6 and 18 h post- $^{32}\text{P}$  application. NC, noncolonized root regions (white bars); BNC, Benomyl-treated noncolonized root region (pink bars); C, colonized root region (yellow bars); BC, Benomyl-treated colonized root region (green bars). Different letters and letters with primes indicate significant differences as determined using Kruskal–Wallis test followed by Dunn's *post hoc* test ( $P < 0.05$ ). The box plots in (e, f) show the lower and upper quartiles, and the minimum and maximum values. The bar in the box represents the median. Each gray point represents the average cpm from one root segment. Measurements at each timepoint and root type combination were collected from more than three root segments.

(Fig. 2). Higher plastidic Pi in these cells could be a result of very active plastid metabolism, including fatty acid biosynthesis to support peri-arbuscular membrane development and to supply lipids to the arbuscule (Bravo *et al.*, 2017; MacLean *et al.*, 2017). A large amount of Pi is produced as a byproduct of ATP hydrolysis during the synthesis of a key precursor Malonyl-CoA (Buchanan *et al.*, 2015) which might contribute to the observed differences.

All experiments involving Pi measurements in the cytosol or plastids included an appropriately targeted Pi-insensitive control sensor, which reports any background, nonspecific FRET changes between cell types or treatments. The control sensor differs from the Pi sensor in just six amino acids in the Pi binding domain (Table S7) (Banerjee *et al.*, 2016) and it has been demonstrated that the control and Pi sensors show equivalent responses to changes in pH and ionic strength (Banerjee *et al.*, 2016). In the majority of our experiments, the control sensor did not fluctuate between treatments or cell types but in a few cases the control sensor registered a significant FRET change, as seen for the epidermal cells following Pi treatment (Fig. 4) indicating a background effect on the sensors. As the FRET change for the

Pi sensor is larger than that of the control sensor, we infer that there is a Pi-dependent component to the FRET response which can be revealed by calculating the difference between the FRET measured by the two sensors. This approach assumes that the unknown background effects on the two sensors are the same, which seems likely given the minor change in protein sequence and the examples of known perturbations pH and ionic strength (Banerjee *et al.*, 2016). Nevertheless, this particular point cannot be proven. Analyte-insensitive control sensors are available only for a few FRET-based sensors but where available, they add considerable experimental value. Display of the control data provides an instant view of background effects for any cell type or treatment comparison and increase confidence in measurements from the sensor (Imamura *et al.*, 2009; Banerjee *et al.*, 2016).

In order to image cells during Pi delivery via the AM fungus, we modified a membrane sandwich growth system (Giovannetti *et al.*, 1993) which constrains mycorrhizal root growth to two dimensions and provides access to the root and hyphae. Using this system, Pi application can be restricted to the ERH and

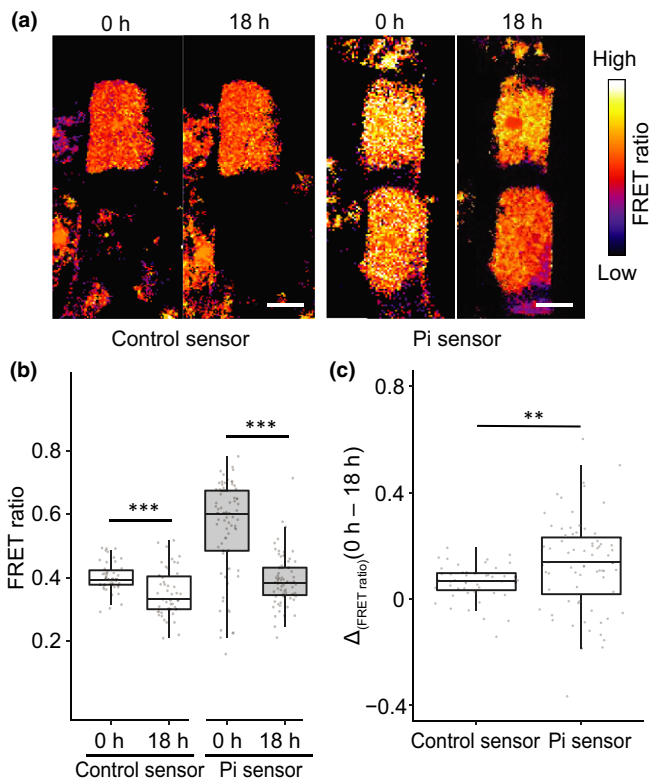


**Fig. 6** Fluorescence resonance energy transfer (FRET) ratios in colonized cells prior to and after local orthophosphate (Pi) application to the extraradical hyphae of *Gigaspora gigantea*. Individual infection units were imaged before (0 h) and after (18 h) Pi feeding. (a) Representative pseudocolor images of FRET ratios from root cells expressing the cytosol-localized sensors before (0 h), and 18 h after local application of Pi to the extraradical hyphae (using the experimental system shown in Fig. 5). Bar, 10  $\mu\text{m}$ . (b) FRET ratios from root cells expressing the cytosol-localized sensors before (0 h), and 18 h after local application of Pi to the extraradical hyphae as in (a). Pairwise Mann–Whitney tests were performed separately for each sensor and significant differences are indicated (\*\*\*,  $P < 0.001$ ). (c) As both sensors showed differences in FRET ratios between treatments, the  $\Delta\text{FRET}$  ratio was calculated using the data in (b). For each sensor, the 18 h mean was subtracted from each 0 h data point. The  $\Delta\text{FRET}$  ratio for the Pi sensor was larger than that of the control sensor (Student's  $t$ -test; \*\*,  $P < 0.01$ ). The box plots in (b, c) show the lower and upper quartiles, and the minimum and maximum values. The bar in the box represents the median. Each gray point in the boxplots represents a measurement from one region of interest (ROI) per cell. Measurements were made on more than 46 cells.

followed by radiotracing and Pi imaging in the colonized cell. The radiotracer experiments indicated significant Pi transfer through the ERH to the root 18 h post-Pi application. Furthermore, the relative Pi content of colonized cells was higher 18 h post-Pi application relative to the pre-Pi application measurement of the same cells. This time frame is similar to previous radiotracer experiments. For example, in *in vitro* carrot root-*Glomus intraradices* associations,  $^{32}\text{P}$ i applied to the ERH was detected in mycorrhizal roots after 14 h (Nielsen *et al.*, 2002), although these experiments do not resolve the cellular location of the Pi. In this same growth system, *Glomus intraradices* Pi transporter transcripts were constitutively present but increased 25-fold within 6 h of Pi application (Maldonado-Mendoza *et al.*,

2001) indicating the potential time frame for increases in transport capacity. Polyphosphate accumulation in the ERH of *Archaeospora leptoticha* was detected just 1 h after P addition to the medium, suggesting that polyphosphate synthesis initiates very quickly (Ezawa *et al.*, 2004). Using  $^{31}\text{P}$ -NMR, polyphosphate signals were detected in the ERH of *Glomus intraradices* 5 h after the addition of P (Viereck *et al.*, 2004), while polyphosphate was estimated to move through the ERH of *Glomus* sp. HR1 at a rate of *c.* 2.0  $\text{mm h}^{-1}$  (Hijikata *et al.*, 2010). While there are differences in the experimental systems as well as the plant–fungus combinations, they are consistent in suggesting that it takes several hours for P movement through the hyphae to the root. Transfer will be influenced by factors in both symbionts, so variation between systems is not surprising (Smith *et al.*, 2004, 2011; Hong *et al.*, 2012). In summary, this experimental setup coupled with plants expressing the Pi biosensor, offers an approach for future exploration of cellular Pi dynamics during symbiosis. Future improvements, including calibration of the Pi sensor in *B. distachyon*, a challenge that has been achieved in *Arabidopsis* (Sahu *et al.*, 2020), would enable absolute measurements of Pi content, and reveal the magnitude of these cellular Pi responses.

## Acknowledgements

Financial support was provided by the US Department of Energy, Office of Science, Office of Biological and Environmental Research (grant no. DE-SC0014037). SZ was supported in part by a NIFA postdoctoral fellowship (#2021-67034-35001). The confocal microscope in the BTI Plant Cell Imaging Center was purchased with a US NSF Instrumentation Grant, DBI-0618969. The authors thank members of WKV's laboratory for helpful discussions and BTI Computational Biology Center for the advice on the Fiji image processor.

## Author contributions

SZ, WKV and MJH designed research; SZ performed research; SZ and MJH analyzed data; DAD, SI, LMM, contributed materials and preliminary imaging method development; LJ, SI and SZ contributed to the IMAGEJ FRET analyzer; SZ and MJH wrote the article; WKV edited the manuscript. DAD, LMM, LJ and SI made equal contributions and are considered equal second co-authors with names listed in alphabetical order.

## ORCID

Dierdra A. Daniels <https://orcid.org/0000-0001-8015-7005>  
 Maria J. Harrison <https://orcid.org/0000-0001-8716-1875>  
 Sergey Ivanov <https://orcid.org/0000-0002-4191-3928>  
 Lena M. Müller <https://orcid.org/0000-0002-6036-4514>  
 Wayne K. Versaw <https://orcid.org/0000-0002-3725-1036>  
 Shiqi Zhang <https://orcid.org/0000-0003-1202-4213>

## Data availability

Data available on request from the authors.

## References

- An J, Zeng T, Ji C, de Graaf S, Zheng Z, Xiao TT, Deng X, Xiao S, Bisseling T, Limpens E *et al.* 2019. A *Medicago truncatula* SWEET transporter implicated in arbuscule maintenance during arbuscular mycorrhizal symbiosis. *New Phytologist* 224: 396–408.
- Arisz SA, Testerink C, Munnik T. 2009. Plant PA signaling via diacylglycerol kinase. *Biochimica et Biophysica Acta* 1791: 869–875.
- Banerjee S, Garcia LR, Versaw WK. 2016. Quantitative imaging of FRET-based biosensors for cell- and organelle-specific analyses in plants. *Microscopy and Microanalysis* 22: 300–310.
- Blancaflor EB, Zhao L, Harrison MJ. 2001. Microtubule organization in root cells of *Medicago truncatula* during development of an arbuscular mycorrhizal symbiosis with *Glomus versiforme*. *Protoplasma* 217: 154–165.
- Bonfante-Fasolo P. 1984. Anatomy and morphology of VA mycorrhizae. In: Powell CL, Bagyaraj DJ, eds. *VA Mycorrhizas*. Boca Raton, FL, USA: CRC Press, 5–33.
- Bragg JN, Anderton A, Nieu R, Vogel JP. 2015. *Brachypodium distachyon*. In: Wang K, ed. *Agrobacterium protocols*. New York, NY, USA: Springer, 17–33.
- Bravo A, Brands M, Wewer V, Dörmann P, Harrison MJ. 2017. Arbuscular mycorrhiza-specific enzymes FatM and RAM2 fine-tune lipid biosynthesis to promote development of arbuscular mycorrhiza. *New Phytologist* 214: 1631–1645.
- Brown RC, Lemmon BE. 1995. Methods in plant immunolight microscopy. *Methods in Cell Biology* 49: 85–107.
- Brundrett MC. 2017. Global diversity and importance of mycorrhizal and nonmycorrhizal plants. In: Tedersoo L, ed. *Biogeography of mycorrhizal symbiosis*. Cham, Switzerland: Springer International, 533–556.
- Buchanan BB, Gruissem W, Jones RL. 2015. *Biochemistry and molecular biology of plants*. Hoboken, NJ, USA: John Wiley & Sons, 465.
- Chiu CH, Paszkowski U. 2019. Mechanisms and impact of symbiotic phosphate acquisition. *Cold Spring Harbor Perspectives in Biology* 11: a034603.
- Choi W-G, Toyota M, Kim S-H, Hilleary R, Gilroy S. 2014. Salt stress-induced  $Ca^{2+}$  waves are associated with rapid, long-distance root-to-shoot signaling in plants. *Proceedings of the National Academy of Sciences, USA* 111: 6497–6502.
- Cox G, Moran KJ, Sanders F, Nockolds C, Tinker PB. 1980. Translocation and transfer of nutrients in vesicular-arbuscular mycorrhizas. III. Polyphosphate granules and phosphorus translocation. *New Phytologist* 84: 649–659.
- Cox G, Sanders F. 1974. Ultrastructure of the host-fungus interface in a vesicular-arbuscular mycorrhiza. *New Phytologist* 73: 901–912.
- Cox G, Tinker PB. 1976. Translocation and transfer of nutrients in vesicular-arbuscular mycorrhizas. *New Phytologist* 77: 371–378.
- Dissanayaka D, Ghahremani M, Siebers M, Wasaki J, Plaxton WC. 2021. Recent insights into the metabolic adaptations of phosphorus-deprived plants. *Journal of Experimental Botany* 72: 199–223.
- Ezawa T, Cavagnaro TR, Smith SE, Smith FA, Ohtomo R. 2004. Rapid accumulation of polyphosphate in extraradical hyphae of an arbuscular mycorrhizal fungus as revealed by histochemistry and a polyphosphate kinase/luciferase system. *New Phytologist* 161: 387–392.
- Floss DS, Gomez SK, Park H-J, MacLean AM, Müller LM, Bhattarai KK, Lévesque-Tremblay V, Maldonado-Mendoza IE, Harrison MJ. 2017. A transcriptional program for arbuscule degeneration during AM symbiosis is regulated by MYB1. *Current Biology* 27: 1206–1212.
- Giovannetti M, Ayio L, Sbrana C, Silvia CA. 1993. Factors affecting appressorium development in the vesicular-arbuscular mycorrhizal fungus *Glomus mosseae* (Nicol. & Gerd.) Gerd. & Trappe. *New Phytologist* 123: 115–122.
- Gu H, Lalonde S, Okumoto S, Looger LL, Scharff-Poulsen AM, Grossman AR, Kossmann J, Jakobsen I, Frommer WB. 2006. A novel analytical method for *in vivo* phosphate tracking. *FEBS Letters* 580: 5885–5893.
- Gu M, Chen A, Sun S, Xu G. 2016. Complex regulation of plant phosphate transporters and the gap between molecular mechanisms and practical application: what is missing? *Molecular Plant* 9: 396–416.
- Gutjahr C, Parniske M. 2013. Cell and developmental biology of arbuscular mycorrhiza symbiosis. *Annual Review of Cell and Developmental Biology* 29: 593–617.
- Harrison MJ, van Buuren ML. 1995. A phosphate transporter from the mycorrhizal fungus *Glomus versiforme*. *Nature* 378: 626–629.
- Harrison MJ, Dewbre GR, Liu J. 2002. A phosphate transporter from *Medicago truncatula* involved in the acquisition of phosphate released by arbuscular mycorrhizal fungi. *Plant Cell* 14: 2413–2429.
- Hijikata N, Murase M, Tani C, Ohtomo R, Osaki M, Ezawa T. 2010. Polyphosphate has a central role in the rapid and massive accumulation of phosphorus in extraradical mycelium of an arbuscular mycorrhizal fungus. *New Phytologist* 186: 285–289.
- Hong JJ, Park Y-S, Bravo A, Bhattarai KK, Daniels DA, Harrison MJ. 2012. Diversity of morphology and function in arbuscular mycorrhizal symbioses in *Brachypodium distachyon*. *Planta* 236: 851–865.
- Imamura H, Nhat KPH, Togawa H, Saito K, Iino R, Kato-Yamada Y, Nagai T, Noji H. 2009. Visualization of ATP levels inside single living cells with fluorescence resonance energy transfer-based genetically encoded indicators. *Proceedings of the National Academy of Sciences, USA* 106: 15651–15656.
- Ivanov S, Harrison MJ. 2014. A set of fluorescent protein-based markers expressed from constitutive and arbuscular mycorrhiza-inducible promoters to label organelles, membranes and cytoskeletal elements in *Medicago truncatula*. *The Plant Journal* 80: 1151–1163.
- Javot H, Penmetsa RV, Terzaghi N, Cook DR, Harrison MJ. 2007. A *Medicago truncatula* phosphate transporter indispensable for the arbuscular mycorrhizal symbiosis. *Proceedings of the National Academy of Sciences, USA* 104: 1720–1725.
- Jiang Y, Wang W, Xie Q, Liu NA, Liu L, Wang D, Zhang X, Yang C, Chen X, Tang D *et al.* 2017. Plants transfer lipids to sustain colonization by mutualistic mycorrhizal and parasitic fungi. *Science* 356: 1172–1175.
- Kanno S, Cuyas L, Javot H, Bligny R, Gout E, Darveville T, Hanchi M, Nakanishi TM, Thibaud MC, Nussaume L. 2016. Performance and limitations of phosphate quantification: guidelines for plant biologists. *Plant and Cell Physiology* 57: 690–706.
- Karimi M, Bleys A, Vanderhaeghen R, Hilson P. 2007. Building blocks for plant gene assembly. *Plant Physiology* 145: 1183–1191.
- Karimi M, De Meyer B, Hilson P. 2005. Modular cloning in plant cells. *Trends in Plant Science* 10: 103–105.
- Keymer A, Pimprikar P, Wewer V, Huber C, Brands M, Bucerius SL, Delaux P-M, Klingl V, Röpenack-Lahaye EV, Wang TL *et al.* 2017. Lipid transfer from plants to arbuscular mycorrhiza fungi. *eLife* 6: e29107.
- Kobayashi Y, Hata S. 2010. Dynamics of periarbuscular membranes visualized with a fluorescent phosphate transporter in arbuscular mycorrhizal roots of rice. *Plant and Cell Physiology* 51: 341–353.
- Kwok E, Hanson M. 2004. Stromules and the dynamic nature of plastid morphology. *Journal of Microscopy* 214: 124–137.
- Lalonde S, Ehrhardt DW, Frommer WB. 2005. Shining light on signaling and metabolic networks by genetically encoded biosensors. *Current Opinion in Plant Biology* 8: 574–581.
- Liu F, Xu Y, Jiang H, Jiang C, Du Y, Gong C, Wang W, Zhu S, Han G, Cheng B. 2016. Systematic identification, evolution and expression analysis of the *Zea mays* PHT1 gene family reveals several new members involved in root colonization by Arbuscular mycorrhizal fungi. *International Journal of Molecular Sciences* 17: 930.
- Liu J, Blaylock LA, Harrison MJ. 2004. cDNA arrays as a tool to identify mycorrhiza-regulated genes: identification of mycorrhiza-induced genes that encode or generate signaling molecules implicated in the control of root growth. *Canadian Journal of Botany* 82: 1177–1185.
- Liu J, Versaw WK, Pumplun N, Gomez SK, Blaylock LA, Harrison MJ. 2008. Closely related members of the *Medicago truncatula* PHT1 phosphate transporter gene family encode phosphate transporters with distinct biochemical activities\*. *Journal of Biological Chemistry* 283: 24673–24681.
- Liu T-Y, Huang T-K, Yang S-Y, Hong Y-T, Huang S-M, Wang F-N, Chiang S-F, Tsai S-Y, Lu W-C, Chiou T-J. 2016. Identification of plant vacuolar transporters mediating phosphate storage. *Nature Communications* 7: 1–11.
- MacLean AM, Bravo A, Harrison MJ. 2017. Plant signaling and metabolic pathways enabling arbuscular mycorrhizal symbiosis. *Plant Cell* 29: 2319–2335.
- Maldonado-Mendoza IE, Dewbre GR, Harrison MJ. 2001. A phosphate transporter gene from the extra-radical mycelium of an arbuscular mycorrhizal fungus *Glomus intraradices* is regulated in response to phosphate in the environment. *Molecular Plant-microbe Interactions* 14: 1140–1148.

- Mukherjee P, Banerjee S, Wheeler A, Ratliff LA, Irigoyen S, Garcia LR, Lockless SW, Versaw WK. 2015. Live imaging of inorganic phosphate in plants with cellular and subcellular resolution. *Plant Physiology* 167: 628–638.
- Nielsen JS, Jøner EJ, Declerck S, Olsson S, Jakobsen I. 2002. Phospho-imaging as a tool for visualization and noninvasive measurement of P transport dynamics in arbuscular mycorrhizas. *New Phytologist* 154: 809–819.
- Novero M, Faccio A, Genre A, Stougaard J, Webb KJ, Mulder L, Parniske M, Bonfante P. 2002. Dual requirement of the LjSym4 gene for mycorrhizal development in epidermal and cortical cells of *Lotus japonicus* roots. *New Phytologist* 154: 741–749.
- Okamoto S, Jones A, Frommer WB. 2012. Quantitative imaging with fluorescent biosensors. *Annual Review of Plant Biology* 63: 663–706.
- Paszowski U, Kroken S, Roux C, Briggs SP. 2002. Rice phosphate transporters include an evolutionarily divergent gene specifically activated in arbuscular mycorrhizal symbiosis. *Proceedings of the National Academy of Sciences, USA* 99: 13324–13329.
- Plaxton WC, Tran HT. 2011. Metabolic adaptations of phosphate-starved plants. *Plant Physiology* 156: 1006–1015.
- Rasmussen N, Lloyd DC, Ratcliffe RG, Hansen PE, Jakobsen I. 2000. <sup>31</sup>P NMR for the study of P metabolism and translocation in arbuscular mycorrhizal fungi. *Plant and Soil* 226: 245–253.
- Rincón-Zachary M, Teaster ND, Sparks JA, Valster AH, Motes CM, Blancaflor EB. 2010. Fluorescence resonance energy transfer-sensitized emission of yellow Cameleon 3.60 reveals root zone-specific calcium signatures in Arabidopsis in response to aluminum and other trivalent cations. *Plant Physiology* 152: 1442–1458.
- Sahu A, Banerjee S, Raju AS, Chiou T-J, Garcia LR, Versaw WK. 2020. Spatial profiles of phosphate in roots indicate developmental control of uptake, recycling, and sequestration. *Plant Physiology* 184: 2064–2077.
- Schachtman DP, Reid RJ, Ayling SM. 1998. Phosphorus uptake by plants: from soil to cell. *Plant Physiology* 116: 447–453.
- Smith SE, Jakobsen I, Grønlund M, Smith FA. 2011. Roles of arbuscular mycorrhizas in plant phosphorus nutrition: interactions between pathways of phosphorus uptake in arbuscular mycorrhizal roots have important implications for understanding and manipulating plant phosphorus acquisition. *Plant Physiology* 156: 1050–1057.
- Smith SE, Smith FA, Jakobsen I. 2003. Mycorrhizal fungi can dominate phosphate supply to plants irrespective of growth responses. *Plant Physiology* 133: 16–20.
- Smith SE, Smith FA, Jakobsen I. 2004. Functional diversity in arbuscular mycorrhizal (AM) symbioses: the contribution of the mycorrhizal P uptake pathway is not correlated with mycorrhizal responses in growth or total P uptake. *New Phytologist* 162: 511–524.
- Versaw WK, Garcia LR. 2017. Intracellular transport and compartmentation of phosphate in plants. *Current Opinion in Plant Biology* 39: 25–30.
- Viereck N, Hansen PE, Jakobsen I. 2004. Phosphate pool dynamics in the arbuscular mycorrhizal fungus *Glomus intraradices* studied by *in vivo* <sup>31</sup>P NMR spectroscopy. *New Phytologist* 162: 783–794.
- Walker N, Smith S. 1984. The quantitative study of mycorrhizal infection: II. The relation of rate of infection and speed of fungal growth to propagule density, the mean length of the infection unit and the limiting value of the fraction of the root infected. *New Phytologist* 96: 55–69.
- Waters MT, Fray RG, Pyke KA. 2004. Stromule formation is dependent upon plastid size, plastid differentiation status and the density of plastids within the cell. *The Plant Journal* 39: 655–667.
- Xie X, Huang W, Liu F, Tang N, Liu Y, Lin H, Zhao B. 2013. Functional analysis of the novel mycorrhiza-specific phosphate transporter AsPT1 and PHT1 family from *Astragalus sinicus* during the arbuscular mycorrhizal symbiosis. *New Phytologist* 198: 836–852.
- Xie X, Lin H, Peng X, Xu C, Sun Z, Jiang K, Huang A, Wu X, Tang N, Salvioli A *et al.* 2016. Arbuscular mycorrhizal symbiosis requires a phosphate transceptor in the *Gigaspora margarita* fungal symbiont. *Molecular Plant* 9: 1583–1608.
- Yang S-Y, Grønlund M, Jakobsen I, Grottemeyer MS, Rentsch D, Miyao A, Hirochika H, Kumar CS, Sundaresan V, Salamin N *et al.* 2012. Nonredundant regulation of rice arbuscular mycorrhizal symbiosis by two members of the PHOSPHATE TRANSPORTER1 gene family. *Plant Cell* 24: 4236–4251.

## Supporting Information

Additional Supporting Information may be found online in the Supporting Information section at the end of the article.

**Fig. S1** Overlay image of a root expressing a plastid-targeted sensor expressed from the BdPT7 promoter.

**Fig. S2** Representative CFP, FRET and Brightfield images showing autofluorescence from *Diversispora epigaea* and *Gigaspora gigantea*.

**Fig. S3** FRET ratios from roots expressing either the control sensor or the Pi sensor in colonized and noncolonized roots.

**Fig. S4** Plastids within a single *Diversispora epigaea*-colonized cell show consistent FRET ratios.

**Fig. S5** A higher magnification view of Fig. 2(b), zone 3 showing morphological differences between stromulated (S) and lens-shaped (L) plastids.

**Fig. S6** An illustration of cells containing distinct arbuscule stages chosen for analyses in Fig. 4.

**Fig. S7** Temporal changes in cytosolic FRET ratios in five cell types following Pi application to *Brachypodium distachyon*/*Diversispora epigaea* mycorrhizal roots.

**Methods S1** IMAGEJ scripts for sensitized FRET analysis.

**Methods S2** IMAGEJ scripts for pseudocolor FRET image generation.

**Table S1** Primers used in this study.

**Table S2** Transgenic lines.

**Table S3** Leica TCS SP5 confocal microscope configurations for Pi imaging.

**Table S4** (a, b) A set of sample data (from Fig. 1a) to demonstrate image analysis procedure.

**Table S5** Significance levels for each time/cell type combination shown in Fig. 4.

**Table S6** <sup>32</sup>Pi diffusion on a wet cellulose membrane.

**Table S7** Biochemical characteristics of cpFLIPi sensors.

Please note: Wiley Blackwell are not responsible for the content or functionality of any Supporting Information supplied by the authors. Any queries (other than missing material) should be directed to the *New Phytologist* Central Office.